Computational Condensed Matter 32 (2022) e00690

Contents lists available at ScienceDirect

Computational Condensed Matter

journal homepage: www.elsevier.com/locate/cocom

Regular article

Exchange-correlation and spin-orbit coupling effects in 18-electrons transparent conductors half-Heusler: Ab-initio study

Djallal Eddine Mellah [a,1], Kamel Demmouche [a,b,*,1]

[a] University of Ain Temouchent Belhadj Bouchaib, B.P. 284, 46000 Ain Temouchent, Algeria
[b] Materials Science and Applications Laboratory, Faculty of Sciences and Technology, University of Ain Temouchent Belhadj Bouchaib, B.P. 284, 46000 Ain Temouchent, Algeria

ARTICLE INFO

Keywords:
Half-Heusler
DFT
SCAN
SOC
GGA

ABSTRACT

The structural and electronic properties of a two non-oxide Transparent Conductors (TC's), Ir-based half-Heusler XIrSb (X = Ti,Zr) are studied using DFT based on plane waves pseudo potential method. We examined two aspects: (i) the effect of the exchange–correlation (XC) approximation, namely: PBE, PBE+U and meta-GGA SCAN (The strongly constrained and appropriately normed); and (ii) the spin–orbit coupling (SOC) effects of the heavy metals on these compounds. We found that: (i) SCAN, similar to PBE+U, yields larger band gap compared to the PBE corresponding values for both compounds. SCAN gives a band gap about halfway between PBE and experiment or Hybrid-GGA. Similarly to PBE and PBE+U, SCAN shows the semiconducting behavior of the compounds with indirect band gap at the same locations in Brillouin Zone; (ii) spin–orbit coupling causes an important splitting in the valence band maximum (VBM) of order 0.44 eV and 0.58 eV for TiIrSb and ZrIrSb respectively leading to reduction of the band gap. Thus, the heavier is the X atom the larger is the SOC splitting. The VBM is dominated by $J_{eff} = 3/2$ state. However, the splitting is almost negligible on the conduction band minimum (CBM). Therefore, SOC is crucial for predicting the band gap and reproducing correctly the electronic structure of these compounds.

1. Introduction

The world today faces great challenges related to energy resources especially in the search for the source of clean energy such as solar energy. Previous scientific researches focused on transparent conducting oxides (TCO's) having a domination over numerous applications. Recently, scientific works predicted new and unexpected 18-electrons half-Heusler (hH) ABX family of compounds manifesting extraordinary functionalities such as thermo-electricity, superconductivity, piezoelectricity and topological insulation [1,2]. Due to their interesting properties these hH compounds have gained popularity and have been widely explored in the last decade [3–11]. Half-Heusler are also relatively less toxic than the well known lead-based thermoelectric materials and exhibit robust mechanical stability [12,13].

Among members of this discovered ABX family four compounds: TiXSb, ZrXSb, TaXGe and TaXSn (X = Ir) were identified as stable transparent hole conductors. These materials have a wide (>2.5 eV) direct band gap for transparency and high hole mobility. The existence of the electronic band gap in half Heusler compounds with 18 valence electrons is explained by d–d hybridization. The participation of d-orbitals is responsible for creating a band gap which is known as d–d band gap. These new functional materials are needed in solar cell, light emitting diode and flat panel display [1,2].

In general the ABX hH with Valence Electron Counts (VEC = 18) compounds are ternary intermetallics made of all metallic AB heavy elements and a heavy X atom in the V–IV group element. The new discovered compound were synthesized by applying the "inverse design principle" [2]. Transparent conductors needed for energy applications represent the usually contraindicated functionalities of optical transparency (electrical insulators) co-existing with electrical conductivity (opaque metals). This discovery opened the way to search transparent conductors among non-oxide heavy-element materials and to designing high-mobility transparent electronic devices.

On the theoretical side, first principles DFT techniques have been performed to examine the thermodynamic stability and the electronic properties of these materials. DFT calculations employed different methodologies with different approximation of exchange–correlation XC. In the seminal works of R. Gautier and F. Yan [1,2] authors used self-consistent hybrid functional exchange–correlation (HSE06) [14,15]

* Correspondence to: BP. 284, 46000 Ain Temouchent, Algeria.
E-mail address: kdemmouche@gmail.com (K. Demmouche).
[1] Authors contributed equally to the research paper.

https://doi.org/10.1016/j.cocom.2022.e00690
Received 9 March 2022; Received in revised form 22 April 2022; Accepted 2 May 2022
Available online 4 July 2022

wave functions within the projector augmented waves (PAW) technique to study the structural and electronic properties of these compounds. They found the half-Heusler 18 electrons compounds to crystallize in cubic (LiAlSi type) structure with space group $F\bar{4}3m$ as illustrated in Fig. 1 for TiIrSb and ZrIrSb and have a band gap between occupied and unoccupied bands that is, non metals. The structure consists of three filled face-centered cubic (fcc) sublattices and one vacant fcc one sublattice consists of interpenetrating three filled interpenetrating cubic (fcc) sublattices and vacant.

There have been several ab-initio studies in the past focusing on the structural, electronic structure and transport properties of these compounds [3–6,11,16,17]. Most of these calculations have been carried out using density functional theory (DFT) within the local density approximation (LDA) or the generalized gradient approximation (GGA), which is known to underestimate the gaps of semiconductors. However, for example to study the influence of the defect or for predicting the thermoelectric properties of a material, one needs a correct description of the electronic structure as well as the gap. For example, hybrid DFT or many-body perturbation theory (MBPT) within the GW approach are found to give excellent agreement with experimentally derived band parameters. But such calculation are computationally expensive approaches especially when dealing with supercell techniques. A popular improved semi-local exchange–correlation at the GGA cost is the Trans–Blaha modified Becke–Johnson potential (TB-mBJ) [18] which is considered as a good approach to reproduce the energy gap more accurately for semiconductors. But this approach is not parameter free and cannot be employed to study the dynamical stability of materials.

The accuracy and efficiency of DFT are provided by the choice of the exchange–correlation (XC) functional. We employed in the present work the recently developed non-empirical meta-GGA functional, called SCAN (strongly constrained and appropriately normed) [19], which has been found to perform better than GGA for calculations of several systems with various types of bonding. It has not been applied previously for the 18-electrons transparent conductors examined in the present work. SCAN provides more accurate crystal volumes and improved band gaps as compared to PBE-GGA [20] for several materials. Often SCAN matches or improves upon the accuracy of a computationally expensive hybrid functionals or GW approach, at almost-GGA cost. It includes also a additional dependence on the kinetic-energy density $\tau(r)$, while GGA approximation depends principally on the local density gradient $\nabla n(r)$. The inclusion enables meta-GGAs to recognize and accordingly treat different chemical bonds (e.g., covalent, metallic, and even weak bonds), which no LDA or GGA can [19]. SCAN was designed so that all the known constraints are satisfied at the semi-local level. The performance of this functional seems up to be very promising for a wide extend of the different problems in materials sciences [21–25]. SCAN can also provide different ground state properties of magnetic ternary Heusler alloys compared to GGA as presented in the work of Ref. [21].

Furthermore, in most previous studies the spin–orbit coupling (SOC) effect in these compounds with heavy elements was not taken into account. However, relativistic effects can play an important role for accurate description of the electronic as well as thermoelectric properties. The inclusion of spin orbit coupling effect corrects the total energy and its derivatives. Thus, it gives a high resolution to understand well the different proprieties of the compounds. This effect increases quickly when the inner-shell electrons are closer to the nucleus as in the heavy atoms. Thus, in this case the SOC effect might increases the kinetic energy of electrons and relativistic effects becomes very important [26]. While in the case of light atoms, the SOC effect is almost neglected or approximated using Dirac equation [27,28]. For TiIrSb and ZrIrSb SOC causes an important splitting in the valence band maximum (VBM) of order 0.44 eV and 0.58 eV respectively. This yields a decrease of the band gap of about 0.15 eV. Formally, our calculations confirmed that SOC has an important role in the electronic structure of XIrSb, especially near the Fermi surface where it causes decreasing band gap and degenerate bands to split, along the high symmetry directions in the Brillouin zone.

We also investigated the importance of SOC for possible formation of a different ground effective angular moment J_{eff} states. As the atomic sites of our compounds have T_d symmetry, the crystal field splits the d orbitals into the T_2 and E states and the p orbitals are in the T_2 state, while the inclusion of SOC splits the 6-fold T_2 degenerate state into higher quartet 4-fold degenerate and lower doubly degenerate states having effective angular momentum $J_{eff} = 3/2$ and $J_{eff} = 1/2$ respectively.

In this work, we carry out systematic calculations on the exchange correlation (XC) and spin–orbit coupling (SOC) effects in the structural stability as well as the electronic properties 18-electrons hH (XIrSb, X = Ti, Zr) compounds. The outline of the paper is as follows. Section 2 is devoted to the description of the computational methods used in the simulations. Section 3 presents the results of the main structural properties, total-energy curves, and structural parameters. In Section 4 the effects of XC and SOC on the electronic structure are discussed by presenting band structure, DOS and PDOS. Conclusions are presented in Section 5.

2. Computational methodology

First-principles calculations of TiIrSb and ZrIrSb Half-Heusler compounds were performed within the density functional theory (DFT) framework using plane wave pseudopotential (PW+PP) formalism as implemented in Quantum Espresso version v.6.7MaX package [29].

The analysis of the structural and electronic properties were performed by mean of the generalized gradient approximation of the exchange–correlation developed by Perdew–Burke–Ernzerhof [20] (GGA-PBE; PBE+U where $U = 3$ eV is used for transition metals in this study [30]). The meta-GGA functional, SCAN, was recently implemented in quantum espresso by Yao and Kanai [24] involving only scalar relativistic pseudopotential.

The pseudo-potentials included in these calculations are USPP (Ultra Soft Pseudo Potential) [31,32] and NCPP (Norm Conserving Pseudo Potential) [33] for PBE and SCAN functional respectively. The following electronic valence configuration is considered: Ti ($3d^2 4s^2$), Zr ($4d^2 5s^2$), Ir ($5d^7 6s^2$), Sb ($5s^2 5p^3$). The valence electron counts yields valence Electron counts VEC = 18 in this case.

For all calculations, the plane-wave basis kinetic-energy cutoff of $E_{cut} = 50$ Ry was applied, whereas the charge-density cutoff ρ_{cut} was kept at 400 Ry. The integration in reciprocal space is performed on the uniform Monkhorst–Pack mesh [34] (MP) of $10 \times 10 \times 10$ k-$points$.

The Half Heusler (XIrSb, X = Ti, Zr) are in cubic LiAlSi-type structures with space group of F = 43 m. As it is illustrated in Fig. 1 The Wykoff positions of the elements are as fellow: X (Ti, Zr) atoms are positioned at $4a(0,0,0)$, Ir atoms occupy $4b(1/4,1/4,1/4)$ and Sb atoms occupy $4c(1/2,1/2,1/2)$.

For different approximations of the XC we performed the calculations in the presence (full relativistic) and absence (scalar relativistic) of the spin orbit coupling (SOC). The effective spin–orbit coupled Hamiltonian is included in the Kohn–Sham DFT calculations. The total Hamiltonian for the Kohn–Sham DFT calculations, including the SOC terms, can be expressed as :

$$\hat{H} = \hat{T} + \hat{V}_{ext} + \hat{V}_{es} + \hat{V}_{Xc} + \hat{H}^{SOC} = \hat{T} + \hat{V}_a + \hat{H}^{SOC} \quad (1)$$

where :

$\hat{T}$: kinetic energy operator
$\hat{V}_{ext}$: external potential operator
$\hat{V}_{es}$: electrostatic or Hartree potential operator
$\hat{V}_{xc}$ :: exchange–correlation potential operator
$\hat{H}^{SOC}$: spin–orbit coupling operator
$\hat{V}_a$: Kohn–Sham potential operator

The Hamiltonian equation for the SOC can be derived from a non relativistic approximation to the Dirac equation [35] by considering the

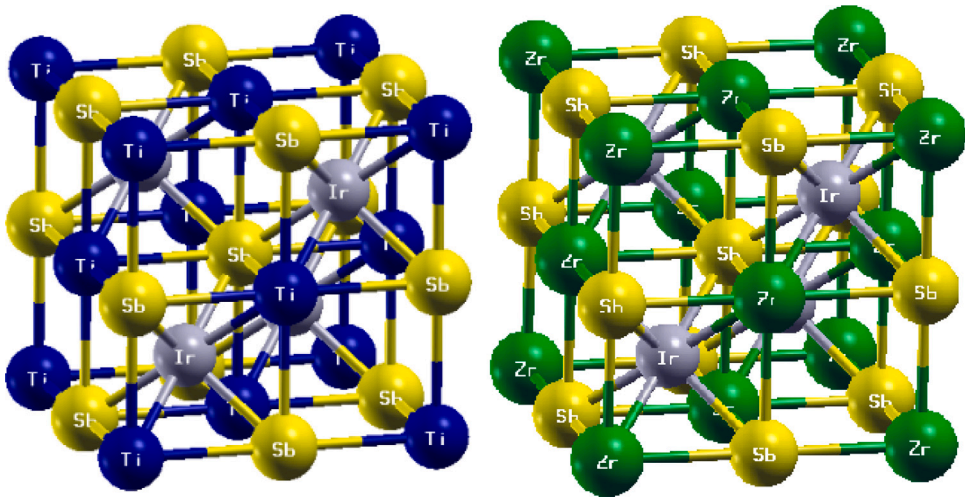

Fig. 1. Structure of XIrSb (X = Ti/Zr) Half-Heusler: left TiIrSb and right ZrIrSb.

relativistic limit as follows: $\hat{H}^{SOC} = \frac{i}{4c^2}(\nabla \hat{V}_a \times \hat{p}).\hat{s}$, where $\hat{p}$ and $\hat{s}$ denote the momentum and spin operators respectively. Considering the central field approximation, $\hat{H}^{SOC}$ becomes:

$\hat{H}^{SOC} = \xi(\hat{r})\hat{l}.\hat{s}$, where $\hat{l}$ is the orbital angular momentum and $\xi(\hat{r}) = \frac{1}{2m^2c^2r}\frac{dV_a}{dr}$ with c being the velocity of light.

3. Structural properties

In this section we calculated the ground states properties of TiIrSb and ZrIrsb by the optimization of their cubic LiAlSi-type structures with space group of $F\bar{4}3m$ using Birch–Murnaghan equation of state [36]. It is given by the following formula:

$$E(V) = E_0 + \frac{9V_0B_0}{16}\left[(\frac{V_0}{V})^{\frac{2}{3}} - 1\right]B_0' + \left[(\frac{V_0}{V})^{\frac{2}{3}} - 1\right]^2\left[6 - 4\left(\frac{V_0}{V}\right)\right] \quad (2)$$

where :

E_0: Equilibrium energy.

V: The unit cell volume.

V_0: The unit cell volume at P = 0 GPa.

B_0: bulk modulus.

B_0': pressure derivative.

The lattice constant a, equilibrium energy E_0, bulk modulus B and its derivative B' at vanishing pressure $P = 0$ GPa were calculated by fitting the total energy (E) as function of volume (V). As it can be seen in Table 1, the obtained values of structural parameters for TiIrSb and ZrIrSb are in good agreement with previous theoretical and experimental data [1,4,5] for all approximations of XC.

The total energy (E) versus volume (V) for the half-Heusler compounds XIrSb (X = Ti/Zr) are plotted in Fig. 2 for different approximations of XC: PBE, PBE+U, SCAN with and without SOC. The equilibrium geometry is determined by minimizing $E(V)$the energy in function of volume where the volume corresponding to the minimum of the $E(V)$ curve is the optimized one while the consequent minimum energy is ground state energy of the unit cell. The lowest energy of the relaxed structure is attained at equilibrium volume V_{eq}, which corresponds to the lattice parameter listed in Table 1 for each approximation used.

Independently of SOC, the results illustrated in 2). show more stable structure in the case of SCAN functional where the total energy is lower than the obtained one in the case of PBE or PBE+U for both compounds Ti/Zr. The optimized lattice parameter is in show a good agreement for TiIrSb and ZrIrSb with previous theoretical and experimental data presented in Table 1. This obtained lattice parameter varies slightly between 6.123A^0 and 6,194A^0 for TiIrSb for SCAN and PBE respectively. For ZrIrSb it varies between 6.306A^0 and 6.379A^0. Thus, the lattice parameter depends upon on the XC functional.

The calculated lattice constants of ZrIrSb compound for each XC functional are about 0.18 A^0 larger than those of the TiIrSb compound. Ir and Sb atoms are the same in the two compounds, hence this result can be easily explained by considering the atomic radii of Zr and Ti : R(Zr) = 1.55 Å, R(Ti) = 1.4 Å. The lattice constant increases with increasing atomic size of the X element in XIrSb compounds. Meanwhile, the bulk modulus B values decrease in the following sequence: B (TiIrSb) > B (ZrIrSb) in inverse sequence of a (the lattice parameter). This outcome is in agreement with the well-known relationship between B and the lattice constants: $B \propto \frac{1}{V_0}$, where V_0 is the unit cell volume. Later, we will discuss how this difference affects the local bonding between different atoms and the resulting electronic structures.

Turning now to SOC influence on structural parameters, the results illustrated in Fig. 2, indicate that the including of SOC extends slightly the total energy for both compounds for all XC approximations. Despite this extension of the total energy, the results in this case show that the structural parameters are not sensible to spin orbit coupling. The lattice parameter values are almost the same when the spin–orbit coupling is erased as shown in Table 1. For these compounds with heavy elements, the SOC has a very minor effect on structural parameters while it plays a vital role in electronic properties as will be discussed in the next section.

4. Electronic properties

We present in this section the band structure calculations of the two compounds XIrSb (X = Ti,Zr) along the directions W-L-Γ-X-W-K in the first BZ. We discuss below in details the effect of the XC functionals as well as the SOC effect on the band structure and the band gap.

4.1. Exchange–correlation (XC) effects on the band structure and energy gap

For all XC approximations the predicted nature of non vanishing band gap is similar. It can be seen that our calculations show that XIrSb (X = Ti,Zr) compounds are an indirect semiconductors as valence band maximum (VBM) and conduction band minimum (CBM) are located at different high symmetry points locations in the IBZ. The indirect gap is from Γ to X as it is shown in all plots in Fig. 3. These results agree well with previous theoretical data [1,2,4–6]. Thus, independently of SOC the results show an increase of the band gap when going from PBE to PBE+U for the two compounds as it can be seen in Table 2. For TiIrSb in the absence of SOC it varies between 0.839 eV and 1.32 eV where this increase is more important than that for the ZrIrSb compounds (1498 eV and 1,517 eV). Thus, in case of Zr the U potential has a small effect

Table 1
The calculated values of lattice constants a, bulk modulus (B), pressure derivative of bulk modulus (B') for XIrSb (X = Ti,Zr) compounds with and without SOC.

	V_{xc}	w/SOC			SOC		
		a (A^0)	B (GPa)	B'	a (A^0)	B (GPa)	B'
TiIrSb	PBE	6.194	147.262	4.542	6.193	146.312	4.556
	PBE+U	6.191	142.818	4.551	6.208	143.635	4.481
	SCAN	6.122	169.467	4.510	6.121	166.956	4.585
	Other	6.114[a]	173.216[d]	4.780[d]			
		6.169[b]	144.820[c]				
		6.116[c]					
		6.162[e]					
ZrIrSb	PBE	6.379	146.167	4.353	6.378	145.383	4.357
	PBE+U	6.374	141.836	4.402	6.371	142.897	4.372
	SCAN	6.306	165.471	4.274	6.304	166.157	4.259
	Other	6.291[a]	167.47[c]	4.76[c]			
		6.372[b]					
		6.299[c]					
		6.328[e]					

[a]Ref [2] Experimental value.
[b]Ref [1] HSE06.
[c]Ref [4,5,11] GGA-PBEsol.
[d]Ref [5,10] TB-mBJ.
[e]Ref [7] GGA+U.

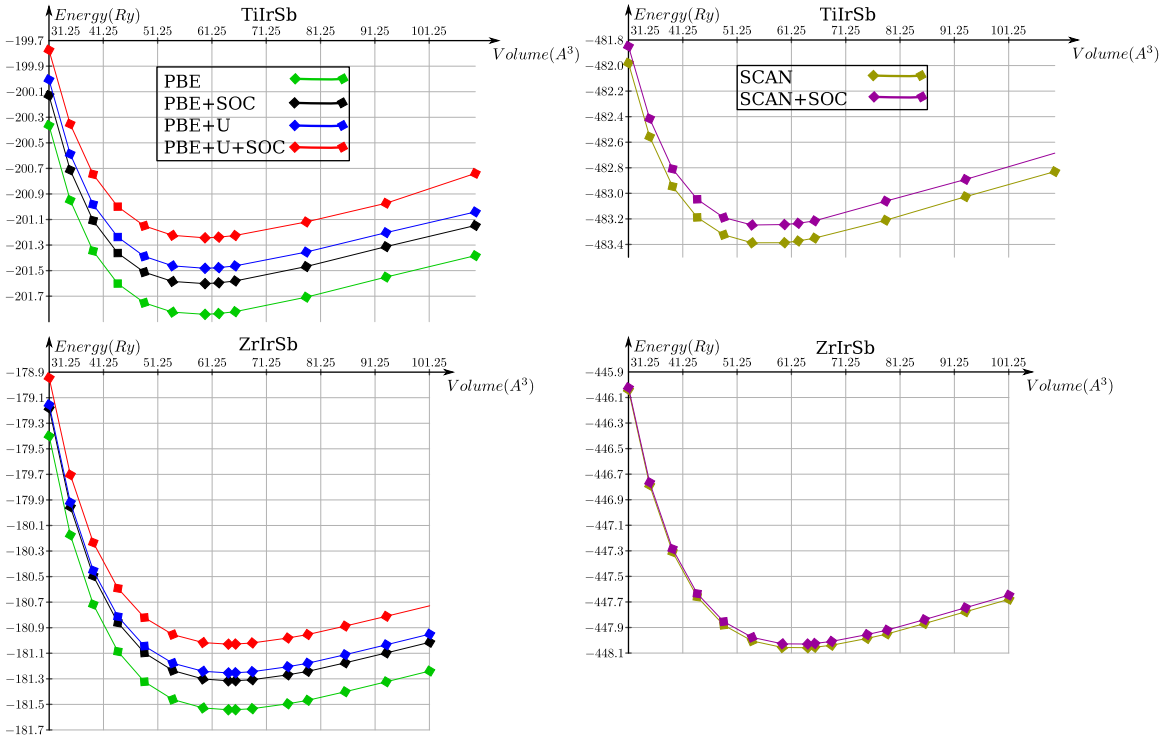

Fig. 2. Energy variation as function of the volume of XIrSb (X = Ti,Zr) half-Heusler compounds.

on the band gap. As it is expected the Hubbard U potential corrects the effects of self-correlation yielding an underestimation of the gap. However, when comparing the calculations using SCAN functional in the absence of SOC we observe a good performance of SCAN (1702 eV) than PBE+U (1.517 eV) for the ZrIrSb compound. In the case of TiIrSb compound it seems that PBE+U (1.242 eV) plays a better role to describe the band gap than SCAN (1.166 eV). The band gap in case of SCAN functional is about half way between PBE and accurate hybrid functional [1]. It performs better than TB-mBJ for example [4,5] at GGA cost. The summary of the energy gaps for the studied compounds for all XC functionals is summarized in histogram type in Fig. 4 and given explicitly in Table 2. These results led us to confirm that the using of SCAN and PBE+U functional gives a better description of the semiconducting behavior of these TC compounds and to the cost of GGA calculations. Compared to the PBE band gap, it is substantially enlarged where both PBE+U and SCAN open the gap between valence and conduction bands to improves the calculated values of band gaps of TiIrSb and ZrIrSb.

4.2. SOC effects on the band gap energy

Independently of XC functionals the spin–orbit coupling has the effect of reducing the gap energy for both compounds. Especially the highest values were obtained in the case of SCAN functional as shown in histograms of Fig. 4. The difference $\triangle = E_g(SOC) - E_g(noSOC)$ between the gap energy calculated with and without SOC is 0.476 eV and 0.542 eV for TiIrSb and ZrIrSb respectively. The values of Δ

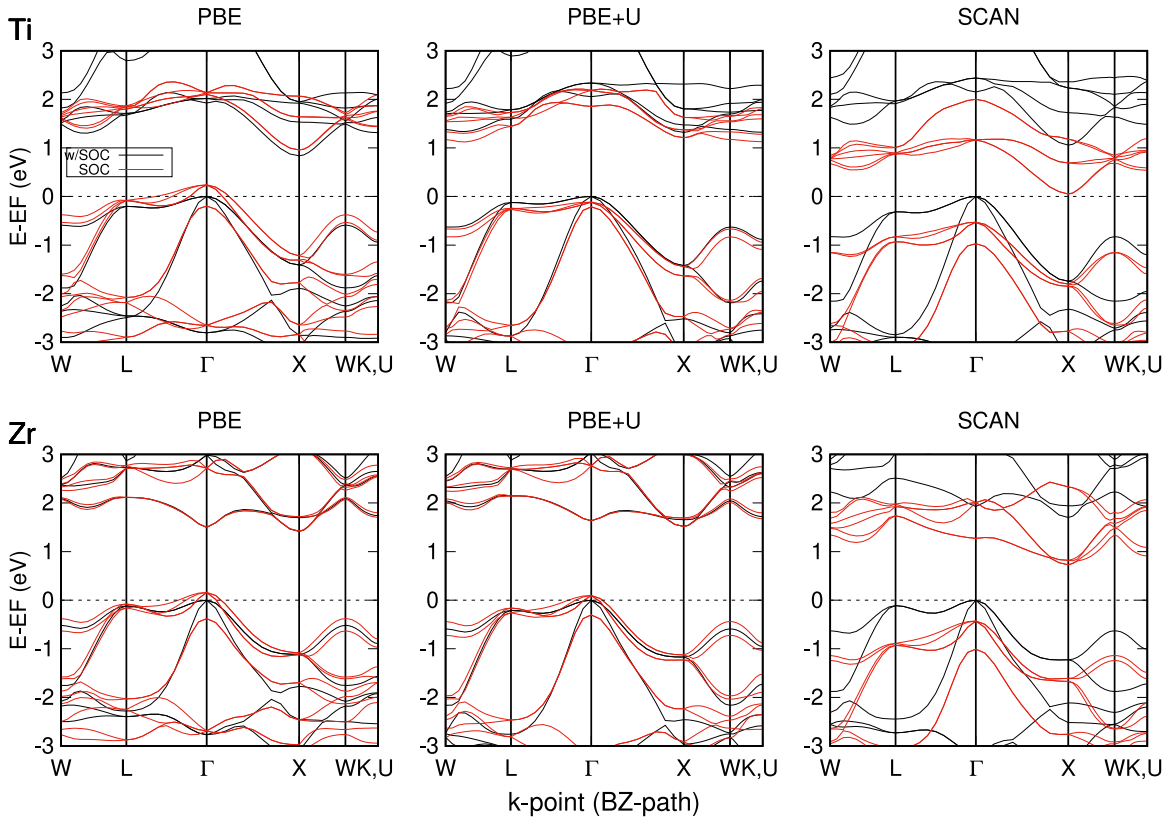

Fig. 3. Calculated band structure for XIrSb (X = Ti and Zr) using (PBE, PBE+U, SCAN) with (Red line) and without (Black line) SOC. (For interpretation of the references to color in this figure legend, the reader is referred to the web version of this article.)

Table 2
Calculated energy gaps (in eV) at high symmetry points for TiIrSb and ZrIrSb.

	Band gap (eV)					
Compound	TiIrSb			ZrIrSb		
Band gap type	Indirect $\Gamma - X$	Direct $\Gamma - \Gamma$	Other $\Gamma - X$	Indirect $\Gamma - X$	Direct $\Gamma - \Gamma$	Other $\Gamma - X$
PBE	0.839	1.926	1.63(HSE06)	1.416	1.498	1.91(HSE06)
PBE+SOC	0.716	1.810	1.11 (mBJ)	1.261	1.339	1.5 (mBJ)
PBE+U	1.321	2.055		1.517	1.631	
PBE+U+SOC	1.242	1.9729		1.418	1.537	
SCAN	1.166	2.149		1.702	1.930	
SCAN+SOC	0.678	1.696		1.16	1.537	

for the other functionals can be viewed from Table 2. We note that we used an indirect method to calculate the band structure in case of SCAN including SOC. We note that SCAN functional calculations turn out to be difficult to perform in the actual quantum espresso version v.6.7MaX. SCAN was recently implemented [24] and can only be used with Norm Conserving pseudo-potentials NCPP, whereas the including of SOC within this functional is not implemented yet. For this reason we tried to perform the calculation in two-steps indirect way using a recipe to obtain an approximate picture of band structure. The first step based on self consistent calculation MetaGGA (SCF-SCAN) with spin polarized (without SOC) on regular **k**-mesh, while the second step is based on a non self consistent calculation (nSCF) GGA including SOC along high symmetry **k**-line. Thus, the expected results from this indirect way is almost the same of GGA+SOC with Norm conserving pseudopotential. So, the obtained values of gap energy including SOC in this present work remain questionable. Therefore, it is necessary to conduct more accurate calculation of this approximation (SCAN) as soon as it is available. It is also possible to utilize an appropriate package where noncollinear calculation for SCAN functional is implemented.

4.3. SOC effects on the band structure

TiIrSb and ZrIrSb are cubic structure where all the atomic sites have T_d symmetry, and thus the crystal field splits the d orbitals into the T_2 and E states and the p orbitals are in the T_2 state, while the SOC creates a 6-fold $J = 5/2$ multiple and a $J = 3/2$ quartet. For our structures Zr/Ti and Ir are nearest neighbors and their $d-$states having same symmetry T_2 or E hybridize with each other. The coupling is strong and the repulsion is responsible for the non vanishing gap and semiconducting nature. At the Γ point the VBM is highest occupied state which is triplet (T_2) degenerate in the absence of SOC as can be seen in Fig. 3 for both compounds. The inclusion of SOC splits the 6-fold T_2 degenerate state into higher quartet 4-fold degenerate and lower doubly degenerate states (see Fig. 3) having effective angular momentum $J_{eff} = 3/2$ and $J_{eff} = 1/2$ respectively (see Ref. [37] for an introduction to effective angular momentum). The SOC effects are similar for the two compounds. The band degeneracy of CBM is not affected by SOC. However, the highest and lower occupied states are shifted upwards and downwards respectively. The value of the SOC splitting for ZrIrSb is greater than that of TiIrSb for all XC functionals

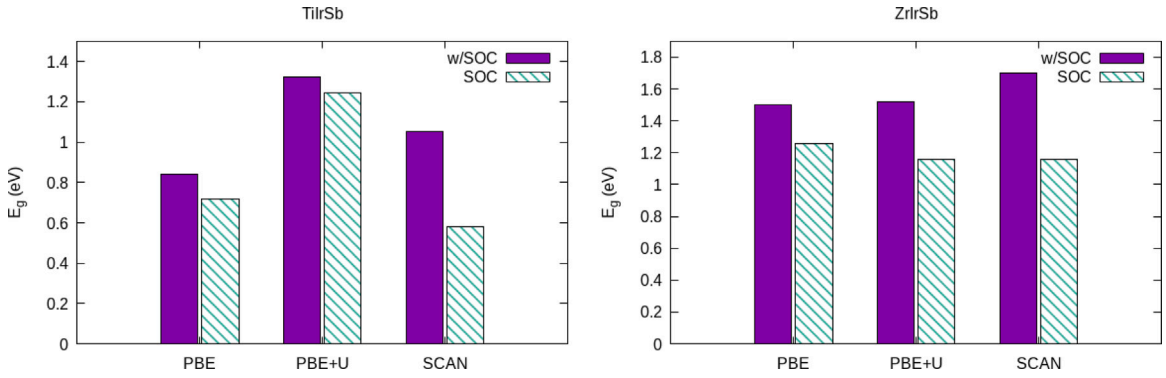

Fig. 4. Comparison of the gap energy in (eV) of XIrSb (X = Ti/Zr) calculated with different exchange–correlation approximations in with and without SOC.

Table 3
Spin–orbit splitting at VBM (in eV) for TiIrSb and ZrIrSb for all functionals.

V_{XC}	Δ_{soc} at VBM (eV)	
	TiIrSb	ZrIrSb
PBE	0.43	0.54
PBE+U	0.10	0.40
SCAN	0.44	0.58

(see Table 3). For example, in case of SCAN functional the value of the splitting is 0.44 eV and 0.58 eV for TiIrSb and ZrIrSb respectively. Since Zr has 5*d* electrons the SOC is more relevant than for the TiIrSb compound having 3*d* electrons for Ir. Moreover, the strength of SOC becomes important for transition metals elements where the Zr atom is heavier than the Ti atom. However, in our systems the heaviest atom is Ir. The dominating states to VBM will be explained in details when combining the band structure and density of states (DOS) calculations in the subsection below. Nevertheless, we note that the highest and the next to highest occupied states at VBM correspond to $J_{eff} = 3/2$ effective angular momentum of Ir-*d*/Ti-*d* mixing state, and $J_{eff} = 1/2$ respectively. This can be confirmed by the PDOS calculations represented in Fig. 5.

Because SOC removes the band degeneracy of VBM rather than that of the CBM, this will affect the Seebeck coefficient and power factor calculation of these thermoelectric materials [8,38]. The thermoelectric properties including SOC effects are subject to our next investigation.

4.4. Density of states (PDOS)

In order to understand the nature of the bonding in the two compounds we performed partial and total density of states calculation (DOS and PDOS) for XIrSb (X = Ti,Zr). Fig. 5 summarizes the calculated PDOS of TiIrSb and ZrIrSb in the energy interval between −8.0 eV and 2.5 eV with all XC approximations: PBE, PBE+U and SCAN. For each XC approximation three PDOS plots are presented: in the upper panel projected DOS of orbital calculated without SOC (w/soc), in below projected DOS with respect to T_2 and E state also without SOC (w/soc-t2g-eg) and in the lower panel projected DOS of orbital calculated in presence of SOC (soc). The Fermi level (E_f) is set to zero energy. Independently of SOC the results show that the structure of valence band arises from the strong hybridization between 3 orbitals Ti/Zr-*d*, Ir-*d* and Sb-*p* for all XC approximations. At valence VBM, Ti/Zr–*d* orbitals in T_2 state have a maximum and more contribution near to the Fermi level, while E states has no relevant contribution. The crystal field causes large $T_2 - E$ splitting in absence of SOC. In the energy interval between −2.0 and −3.5 eV, the sharp peaks derived from Ir-d orbitals by the high contribution of T_2 and E states. The domination of Ir-d in this interval is similar for both compounds and for all XC approximations. However, the contribution of Ir-*d* E states becomes almost zero in the range of −3.5 to −4.5 eV, while T_2 states of Ir-*d* orbital remains more dominant with a less contribution of Sb-*p* orbital in T_2 state for TiIrSb and ZrIrSb compounds. The Sb-*p* in T_2 state shows a maximum and high contribution in the range of −4.5 to −6 eV for all approximations.

In the absence of SOC, the structure of conduction band in the energy interval between CBM and 2.5 eV is dominated by Ti-*d*/Zr-*d* orbitals in T_2 and E states. For TiIrSb Ti-*d* orbitals in E state contribute principally to CBM as shown by the calculated PDOS for PBE and SCAN functional. Whereas, the contribution of T_2 state is weak. However, in the case of PBE+U functional T_2 state dominate over E state. The effect of Hubbard potential U on Ti-d orbitals in T_2 state causing strong hybridization with Ir-*d* orbitals. For ZrIrSb compound, the calculated PDOS show that CBM is dominated by Zr-*d* states in T_2 and E states. T_2 state has higher contribution than E state for all XC approximations.

SOC splits T_2 states into effective total angular momentum $J_{eff} = 1/2$ (doublet) and $J_{eff} = 3/2$ (quartet) states which branched off from $J = 3/2$ and $J = 5/2$ respectively (see Fig. 5). The calculated PDOS in the presence of SOC for all XC approximations show a dominance of $J = 5/2$ and $J = 3/2$ states of Ti/Zr-*d* orbitals at CBM. Thus, the CBM arises from the dominance of highest occupied states Ti-*d*/Zr-*d* states, while VBM is originated principally from the mixing of highest occupied states Ti-*d*/Ir-*d*. The strong SOC leads to the appearance of new peaks in PDOS along the valence band for both compounds in the range of −1.5 eV to −2.5 eV in the case of PBE and from −2 eV to −3.5 eV in the case of PBE+U and from −2.5 eV to −3.7 eV for SCAN. These sharp peaks are originated from high contribution of Ir-*d* in $J = 5/2$ state (having effective angular momentum $J_{eff} = 3/2$). The other intermediate peaks show a dominance of $J = 3/2$ states (having effective angular momentum $J_{eff} = 1/2$). However, in the lower energy range PDOS show a sharp peak dominated by $J = 3/2$ states of Sb-p orbitals with less contribution of $J = 3/2$ states of Ir-*d* orbitals for the two compounds for all XC approximations.

5. Conclusion

The novelty of this study revolves around the importance of spin orbit coupling (SOC) and exchange correlation (XC) to determine structural and electronic proprieties of the two transparent conducting 18-electron half-Heusler Ir-based compounds TiIrSb and ZrIrSb. Especially with regard to band gap and band structure. To investigate that, we performed DFT calculations using different XC approximations, namely: PBE, PBE+U and SCAN functional in the presence and in the absence of SOC.

For the correlation effects we focus on the recently developed meta-GGA, SCAN. It has been found to perform better than standard GGA for the calculations of several systems. SCAN within pseudopotential methodology is viewed as a correction of PBE containing extra semilocal information and has been recently implemented in Quantum Espresso (QE). Moreover, SCAN is a promising XC functional, which

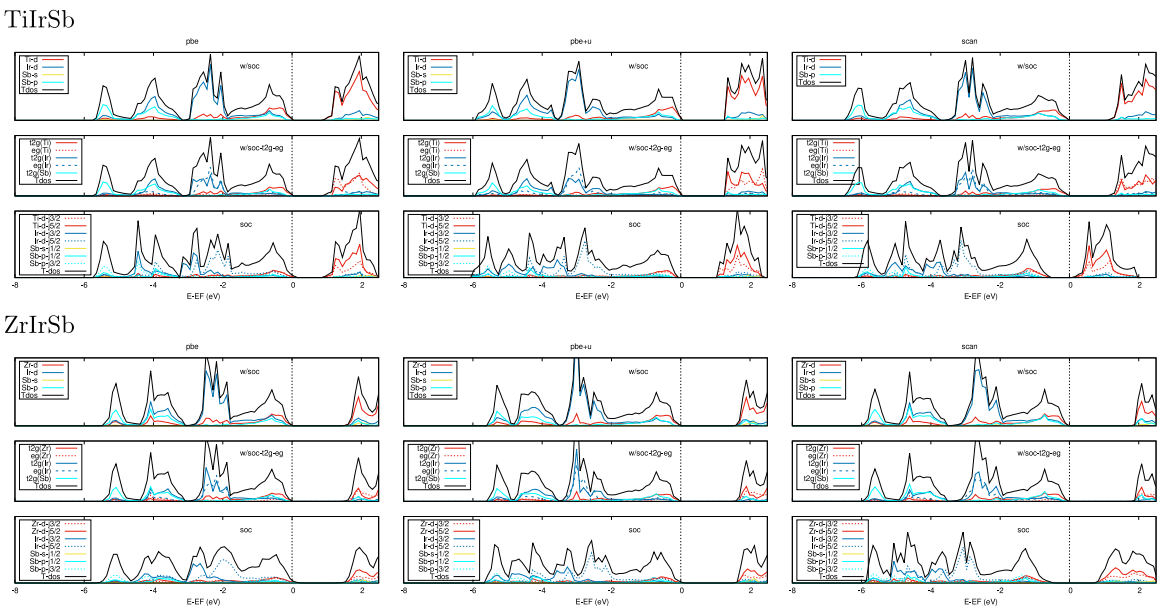

Fig. 5. The total and partial density of states within PBE, PBE+U, SCAN approximations for TiIrSb and ZrIrSb with and without SOC.

at low costs, can describe defects in TiIrSb and ZrIrSb compounds compared to hybrid functionals. We know that standard functionals like PBE fail to show the defect levels inside the band gap.

The present investigation suggests that correlation corrections beyond GGA are rather minor for the lattice parameters of TiIrSb and ZrIrSb compounds. The calculation of lattice parameters are in excellent agreement with previous theoretical and experimental data ones for both compounds for all XC approximations. However, significant differences between GGA and meta-GGA can be observed for the bulk moduli calculation. Moreover, the effect of the inclusion of the spin–orbit coupling is almost negligible on the structural properties such as the lattice parameters where the obtained values in this case are almost the same as those obtained in the calculation not including SOC.

The electronic structure shows a semiconducting behavior of XIrSb (X = Ti/Zr) with indirect band gap. The calculated band gap shows an increase of the gap energy E_g when going from PBE to PBE+U for the two compounds. This increase is more important in the case of TiIrSb than of ZrIrSb. However, the calculations using SCAN show a good performance than PBE and PBE+U in the case of ZrIrSb, while it seems that PBE+U plays a better role to describe the band gap than SCAN for the case of TiIrSb. This suggests that in general SCAN and GGA+U calculations will be an effective tool for narrow gap HH semiconductors.

The presence of spin–orbit coupling reduces the gap energy for both compounds. This reduction of the band-gap is larger in case of SCAN than in the case of the other XC approximations where the difference is of order 0.476 eV and 0.542 eV for TiIrSb and ZrIrSb respectively. The spin–orbit coupling causes an important splitting in the valence band maximum (VBM) of order 0.44 eV and 0.58 eV for TiIrSb and ZrIrSb respectively. However, these two values remain questionable due to the indirect way we used for SCAN+SOC calculation as indicated above (see Section 4.2). The strong coupling causes a band splitting at VBM, where it splits the 6-fold T_2 degenerate state into higher quartet 4-fold degenerate and lower doubly degenerate states having effective angular momentum $J_{eff} = 3/2$ and $J_{eff} = 1/2$ respectively. It is worth mentioning that SOC splitting is greater for ZrIrSb than for TiIrSb. This is due to its strong effect on transition metals elements in XIrSb compounds where the X = Zr atom is heavier than the X = Ti atom. In the other hand, the band degeneracy of CBM is not affected by SOC. However, the highest occupied and the lowest unoccupied states are shifted upwards and downwards respectively.

The calculation PDOS led us to understand well the nature of the bonding in the two compounds where the results showed a high contribution of Ti-d/Ir-d and Zr-d/Ir-d states at VBM for TiIrSb and ZrIrSb whereas CBM is dominated principally by Ti/Zr-d states

Finally, regardless of the XC approximation it is relevant to include the SOC when studying the 18 electrons half Heusler transparent conductors. Especially, for extended systems such as defective structures. In the other hand, SCAN provides more accurate and improved band gaps as compared to standard GGA. We believe that we would use the SCAN approximation to describe point defect in these transparent conducting compounds in our next investigation.

Declaration of competing interest

The authors declare that they have no known competing financial interests or personal relationships that could have appeared to influence the work reported in this paper.

Data availability

Data will be made available on request.

References

[1] G. Romain, Z. Xiuwen, H. Linhua, Y. Liping, L. Yuyuan, S. Tor, C. Danbee, P.K. R., Z. Alex, Prediction and accelerated laboratory discovery of previously unknown 18-electron ABX compounds, Nature Chem. 7 (2015) 308–316, http://dx.doi.org/10.1038/nchem.2207.

[2] Y. Feng, Z. Xiuwen, G. Yu Yonggang, Y. Liping, N. Arpun, O. Mason Thomas, Z. Alex, Design and discovery of a novel half-Heusler transparent hole conductor made of all-metallic heavy elements, Nature Commun. 6 (2015) 7308, http://dx.doi.org/10.1038/ncomms8308.

[3] S. Anand, K. Xia, V. I. Hegde, U. Aydemir, V. Kocevski, T. Zhu, C. Wolverton, G.J. Snyder, A valence balanced rule for discovery of 18-electron half-Heuslers with defects, Energy Environ. Sci. 11 (2018) 1480–1488, http://dx.doi.org/10.1039/C8EE00306H.

[4] B. Yassine, A. Kadda, D. Bendouma, A. Omar, Z. Mostefa, B. B., M. Allel, Structural stability, electronic structure, and novel transport properties with high thermoelectric performances of ZrIrX (X=As, Bi, and Sb), J. Electron. Mater. 16 (2017) 1–11, http://dx.doi.org/10.1007/s10825-016-0937-8.

[5] S. Chibani, O. Arbouche, M. Zemouli, K. Amara, Y. Benallou, Y. Azzaz, B. Belgoumene, A. Bentayeb, M. Ameri, Ab initio prediction of the structural, electronic, elastic, and thermoelectric properties of half-Heusler ternary compounds TiIrX (X=As and Sb), J. Electron. Mater. 47 (2018) 196–204, http://dx.doi.org/10.1007/s11664-017-5761-9.

[6] K. Kaur, R. Kumar, Ti based half Heusler compounds: A new on the screen with robustic thermoelectric performance, J. Alloys Compd. 727 (2017) 1171–1177, http://dx.doi.org/10.1016/j.jallcom.2017.08.216, URL https://www.sciencedirect.com/science/article/pii/S0925838817329456.

[7] M. Zhong, W. Zeng, F.-S. Liu, B. Tang, Q.-J. Liu, Explanation for the conductivity difference of half-Heusler transparent conductors via ionization energy, Phys. Chem. Chem. Phys. 23 (2021) 9285–9293, http://dx.doi.org/10.1039/D1CP00382H.

[8] J. Wei, G. Wang, Properties of half-Heusler compounds TaIrGe by using first-principles calculations, Appl. Phys. A 123 (2017) 375, http://dx.doi.org/10.1007/s00339-017-0990-6.

[9] H. Joshi, D.P. Rai, A. Laref, R.K. Thapa, Electronic, and thermoelectric properties of half-heusler compounds MCoSb (M=Ti, Zr, Hf): a first principles study, 6 (6) (2019) 066307, http://dx.doi.org/10.1088/2053-1591/ab0c68.

[10] M. Zhang, J. Wei, G. Wang, Thermoelectric and topological properties of half-Heusler compounds ZrIrX(As, Sb, Bi), Phys. Lett. A 382 (9) (2018) 673–678, http://dx.doi.org/10.1016/j.physleta.2018.01.007, URL https://www.sciencedirect.com/science/article/pii/S0375960118300331.

[11] M.K. Bamgbose, First-principles study of electronic structure and thermoelectric properties of p-type XIrSb(X=Ti, Zr and Hf) half-Heusler compounds, Mater. Sci. Semicond. Process. 129 (2021) 105792, http://dx.doi.org/10.1016/j.mssp.2021.105792, URL https://www.sciencedirect.com/science/article/pii/S1369800121001311.

[12] S. Ouardi, G.H. Fecher, C. Felser, M. Schwall, S.S. Naghavi, A. Gloskovskii, B. Balke, J. Hamrle, K. Postava, J.r. Pištora, S. Ueda, K. Kobayashi, Electronic structure and optical, mechanical, and transport properties of the pure, electron-doped, and hole-doped Heusler compound CoTiSb, Phys. Rev. B 86 (2012) 045116, http://dx.doi.org/10.1103/PhysRevB.86.045116, URL https://link.aps.org/doi/10.1103/PhysRevB.86.045116.

[13] L. Guodong, et al., Enhanced ideal strength of thermoelectric half-Heusler TiNiSn by sub-structure engineering, J. Mater. Chem. A 4 (2016) 14625–14636, http://dx.doi.org/10.1039/C6TA04123J.

[14] J. Heyd, G.E. Scuseria, M. Ernzerhof, Hybrid functionals based on a screened Coulomb potential, J. Chem. Phys. 118 (18) (2003) 8207–8215, http://dx.doi.org/10.1063/1.1564060.

[15] J. Heyd, G.E. Scuseria, M. Ernzerhof, Erratum: Hybrid functionals based on a screened Coulomb potential [J. Chem. Phys. 118, 8207 (2003)], J. Chem. Phys. 124 (21) (2006) 219906, http://dx.doi.org/10.1063/1.2204597.

[16] T. Fang, X. Zhao, T. Zhu, Band structures and transport properties of high-performance half-Heusler thermoelectric materials by first principles, Materials 11 (5) (2018) http://dx.doi.org/10.3390/ma11050847, URL https://www.mdpi.com/1996-1944/11/5/847.

[17] H. Joshi, D. Rai, L. Hnamte, A. Laref, R. Thapa, A theoretical analysis of elastic and optical properties of half Heusler MCoSb (M=Ti, Zr and Hf), Heliyon 5 (3) (2019) e01155, http://dx.doi.org/10.1016/j.heliyon.2019.e01155, URL https://www.sciencedirect.com/science/article/pii/S2405844018376072.

[18] F. Tran, P. Blaha, Accurate band gaps of semiconductors and insulators with a semilocal exchange-correlation potential, Phys. Rev. Lett. 102 (2009) 226401, http://dx.doi.org/10.1103/PhysRevLett.102.226401, URL https://link.aps.org/doi/10.1103/PhysRevLett.102.226401.

[19] J. Sun, A. Ruzsinszky, J.P. Perdew, Strongly constrained and appropriately normed semilocal density functional, Phys. Rev. Lett. 115 (2015) 036402, http://dx.doi.org/10.1103/PhysRevLett.115.036402, URL https://link.aps.org/doi/10.1103/PhysRevLett.115.036402.

[20] J.P. Perdew, K. Burke, M. Ernzerhof, Generalized gradient approximation made simple, Phys. Rev. Lett. 77 (1996) 3865–3868, http://dx.doi.org/10.1103/PhysRevLett.77.3865, URL https://link.aps.org/doi/10.1103/PhysRevLett.77.3865.

[21] V.D. Buchelnikov, V.V. Sokolovskiy, O.N. Miroshkina, M.A. Zagrebin, J. Nokelainen, A. Pulkkinen, B. Barbiellini, E. Lähderanta, Correlation effects on ground-state properties of ternary Heusler alloys: First-principles study, Phys. Rev. B 99 (2019) 014426, http://dx.doi.org/10.1103/PhysRevB.99.014426, URL https://link.aps.org/doi/10.1103/PhysRevB.99.014426.

[22] B. Himmetoglu, V.M. Katukuri, M. Cococcioni, Origin of magnetic interactions and their influence on the structural properties of Ni2MnGa and related compounds, J. Phys.: Condens. Matter 24 (18) (2012) 185501, http://dx.doi.org/10.1088/0953-8984/24/18/185501.

[23] P.J. Hasnip, J.H. Smith, V.K. Lazarov, Ab initio studies of disorder in the full Heusler alloy Co2FexMn1xSi, J. Appl. Phys. 113 (17) (2013) 17B106, http://dx.doi.org/10.1063/1.4801745, arXiv:10.1063/1.4801745.

[24] Y. Yao, Y. Kanai, Plane-wave pseudopotential implementation and performance of scan meta-GGA exchange-correlation functional for extended systems, J. Chem. Phys. 146 (22) (2017) 224105, http://dx.doi.org/10.1063/1.4984939, arXiv:10.1063/1.4984939.

[25] M. Chen, H.-Y. Ko, R.C. Remsing, M.F. Calegari Andrade, B. Santra, Z. Sun, A. Selloni, R. Car, M.L. Klein, J.P. Perdew, X. Wu, Ab initio theory and modeling of water, Proc. Natl. Acad. Sci. 114 (41) (2017) 10846–10851, http://dx.doi.org/10.1073/pnas.1712499114, arXiv:https://www.pnas.org/content/114/41/10846.full.pdf.

[26] M.J. Verstraete, M. Torrent, F. Jollet, G. Zérah, X. Gonze, Density functional perturbation theory with spin-orbit coupling: Phonon band structure of lead, Phys. Rev. B 78 (2008) 045119, http://dx.doi.org/10.1103/PhysRevB.78.045119, URL https://link.aps.org/doi/10.1103/PhysRevB.78.045119.

[27] L. Visscher, T. Saue, Approximate relativistic electronic structure methods based on the quaternion modified Dirac equation, J. Chem. Phys. 113 (10) (2000) 3996–4002, http://dx.doi.org/10.1063/1.1288371, arXiv:10.1063/1.1288371.

[28] C.L. Kane, E.J. Mele, Quantum spin Hall effect in graphene, Phys. Rev. Lett. 95 (2005) 226801, http://dx.doi.org/10.1103/PhysRevLett.95.226801, URL https://link.aps.org/doi/10.1103/PhysRevLett.95.226801.

[29] P. Giannozzi, O. Baseggio, P. Bonfà, D. Brunato, R. Car, I. Carnimeo, C. Cavazzoni, S. de Gironcoli, P. Delugas, F. Ferrari Ruffino, A. Ferretti, N. Marzari, I. Timrov, A. Urru, S. Baroni, Quantum ESPRESSO toward the exascale, J. Chem. Phys. 152 (15) (2020) 154105, http://dx.doi.org/10.1063/5.0005082, arXiv:10.1063/5.0005082.

[30] E. Shatsala, M. Mageto, G. Manyali, M. Mghendi, Thermodynamic stability of ABX heavy elements of TaIrGe, TiIrSb, TaIrSn and ZrIrSb TCOs using the half-Heusler technique, Energy Procedia 93 (2016) http://dx.doi.org/10.1016/j.egypro.2016.07.169.

[31] D. Vanderbilt, Soft self-consistent pseudopotentials in a generalized eigenvalue formalism, Phys. Rev. B 41 (1990) 7892–7895, http://dx.doi.org/10.1103/PhysRevB.41.7892, URL https://link.aps.org/doi/10.1103/PhysRevB.41.7892.

[32] K. Laasonen, R. Car, C. Lee, D. Vanderbilt, Implementation of ultrasoft pseudopotentials in ab initio molecular dynamics, Phys. Rev. B 43 (1991) 6796–6799, http://dx.doi.org/10.1103/PhysRevB.43.6796, URL https://link.aps.org/doi/10.1103/PhysRevB.43.6796.

[33] D.R. Hamann, Optimized norm-conserving vanderbilt pseudopotentials, Phys. Rev. B 88 (2013) 085117, http://dx.doi.org/10.1103/PhysRevB.88.085117, URL https://link.aps.org/doi/10.1103/PhysRevB.88.085117.

[34] H.J. Monkhorst, J.D. Pack, Special points for Brillouin-zone integrations, Phys. Rev. B 13 (1976) 5188–5192, http://dx.doi.org/10.1103/PhysRevB.13.5188, URL https://link.aps.org/doi/10.1103/PhysRevB.13.5188.

[35] L.L. Foldy, S.A. Wouthuysen, On the Dirac theory of spin 1/2 particles and its non-relativistic limit, Phys. Rev. 78 (1950) 29–36, http://dx.doi.org/10.1103/PhysRev.78.29, URL https://link.aps.org/doi/10.1103/PhysRev.78.29.

[36] F.D. Murnaghan, The compressibility of media under extreme pressures, Proc. Natl. Acad. Sci. 30 (9) (1944) 244–247, http://dx.doi.org/10.1073/pnas.30.9.244, arXiv:https://www.pnas.org/content/30/9/244.full.pdf.

[37] M. Xing, Y. Kunihiko, O. Tamio, P. Silvia, Metal-insulator transition and Jeff=1/2 spin-orbit insulating state in rutile-based IrO2/TiO2 superlattices, 2017, arXiv 2017, arXiv:1702.04408.

[38] D. Hoat, M. Naseri, Electronic and thermoelectric properties of RbYSn half-Heusler compound with 8 valence electrons: Spin-orbit coupling effect, Chem. Phys. 528 (2020) 110510, http://dx.doi.org/10.1016/j.chemphys.2019.110510, URL https://www.sciencedirect.com/science/article/pii/S0301010419306263.